Chemistry Africa (2023) 6:1515–1528
https://doi.org/10.1007/s42250-023-00586-7

ORIGINAL ARTICLE

The Removal Efficiency of Cadmium (Cd^{2+}) and Lead (Pb^{2+}) from Aqueous Solution by Graphene Oxide (GO) and Magnetic Graphene Oxide (α-Fe_2O_3/GO)

M. Kadari[1,2] · M. Makhlouf[1,2] · O. Ould Khaoua[1] · M. Kesraoui[1] · S. Bouriche[2] · Z. Benmaamar[2]

Received: 11 September 2022 / Accepted: 3 January 2023 / Published online: 7 January 2023

Abstract
In this study, the modified Hummer method was used to prepare graphene oxide (GO) and magnetic graphene oxide (α-Fe_2O_3/GO). The as-obtained Go and α-Fe_2O_3/GO were characterized using Fourier Transform Infrared, Raman spectroscopy, X-ray diffraction, and Brunauer Emmett Teller. The adsorptive capacity of these materials towards cadmium (Cd^{2+}) and lead (Pb^{2+}) has been studied. An adsorption process with regeneration was carried out, such as equilibrium time, effect of the initial concentration of Cd^{2+} and Pb^{2+}, effect of the amount of the GO, and α-Fe_2O_3/GO and pH effect. The adsorption of an aqueous solution of Cd^{2+} and Pb^{2+} with an initial concentration of 10^{-3} M of the two heavy metals onto 0.1 g of the prepared materials reached an equilibrium time in 2 h with an adsorption rate of more than 90% for both metals. The fine morphology of the adsorbents facilitated the rapid diffusion of the metals studied in the pores, which increased the kinetic. The kinetics can be described by the pseudo-second-order model with $R^2 = 0.993$ and $R^2 = 0.997$ for Cd^{2+} and Pb^{2+}, respectively. The thermodynamic study reveals that the adsorption process is spontaneous, exothermic, and random as temperature increases. The adsorption mechanism included physical adsorption, ion exchange and possibly surface complexation. According to the results obtained and the ease of obtaining α-Fe_2O_3/GO, we can say that it is a promising adsorbent for Cd^{2+} and Pb^{2+}. The magnetic nanoparticle α-Fe_2O_3/GO can be recovered using a magnet. As a result, it is a reusable and recyclable adsorbent.

Keywords Graphene oxide · α-Fe_2O_3/GO · Cd^{2+} · Pb^{2+} · Adsorption

1 Introduction

In recent years, an increasing interest has been observed on an international scale concerning the aquatic pollution caused by toxic metals coming directly from human activities [1–3]. In countries with high industrial concentrations, heavy metals released into nature are a major source of toxicity for the aquatic ecosystem, which causes a lot of concern among the population [4, 5]. Indeed, these heavy metals are the cause of many health problems [6].

Wastewater that contains heavy metals comes from several sources [7, 8]. The surface treatment industry (electroplating) is the one that releases the most heavy metals into solution [9–11]. It produces the most wastewater with cadmium [12], lead [13], nickel [14], chrome [15], zinc [16], and copper concentrations greater than 1 mg/L [17].

Other industries are also responsible for the contamination of wastewater by heavy metals: foundries [18], petroleum refineries [19], the paint industry [20], ink and associated products [21]. Due to the strict control of discharges of wastewater containing heavy metal ions into the environment, practical solutions are needed. To overcome these problems, researchers have concentrated their efforts on the development of treatment methods (physicochemical and biological processes) [22, 23] and disposal of this toxic waste.

Treatment methods such as chemical precipitation [24, 25], electrodeposition [26], ion exchange [27], membrane separation [26], reverse osmosis [28], oxidation–reduction, evaporation, and solvent extraction are all techniques that are still used today [29].

✉ M. Kadari
mohamed_msma@yahoo.fr

1 Combustion, Detonation and Ballistics Research Laboratory, AMC, Tipaza, Algeria

2 Energy and Nanotechnology Processes Laboratory ex FUNDPAL, University of Blida, Blida, Algeria

Depollution techniques, in particular those using chelating resins allowing the selective fixation of heavy metals [30], have also been widely demonstrated and touted as applicable technologies. The use of microorganisms [31, 32] to remove metal ions in solutions has also been studied for a long time. Depending on the nature of the aqueous effluents and the concentrations of metal ions, the industrial application of these processes is restricted, either because of the operating costs or because of the ineffectiveness of the technique to achieve a degree of purification respecting water quality standards [33].

The appearance of new so-called "clean" technology [34] makes it possible to solve a large part of all the problems inherent in the treatment of wastewater containing metals.

Graphite-based inorganic materials, such as Graphene oxide GO and magnetized Graphene oxide α-Fe_2O_3/GO can be used as metal cation adsorbents [35–37]. However, one of the serious drawbacks of the use of GO is the presence of the latter in the treated wastewater due to insufficient filtration and centrifugation processes for its separation [38]. Magnetization of graphene oxide as a simple method for the separation of nano-pollutants such as cadmium (Cd^{2+}) and lead (Pb^{2+}) becomes highly desirable in wastewater treatment [39–42]. This is an efficient technique for recovering magnetic nanoparticles using a magnet and this makes α-Fe_2O_3/GO as a reusable and recyclable adsorbent.

Several techniques have been reported in the literature in recent years for the synthesis of magnetite nanoparticles α-Fe_2O_3, such as thermal decomposition [43], solvothermy, micro-emulsion [44], sono-chemistry, chemical vapor deposition, microwaves [45], hydrothermal energy, photolysis, sol–gel [46], and electrochemical processes [47–49].

Graphene oxide (GO) is widely used because of its long-lasting properties, which make it an excellent adsorbent material for removing dyes and heavy metals. Despite these properties, when using GO as an adsorbent, some problems arise, such as difficult recycling and irreversible aggregation on its surface, resulting in poor performance. To address these issues, graphene oxide has been chemically reacted with other materials such as clay, polymers, and zeolites. The primary goal of this research is to study the performance of magnetized graphene oxide α-Fe_2O_3/GO as a substituent of graphene oxide GO for the retention of cadmium (Cd^{2+}) and lead (Pb^{2+}) in polluted waters thanks to its ease of recovery. By demonstrating the potential and viability of magnetized graphene oxide α-Fe_2O_3/GO for the removal of existing cadmium and lead in contaminated water, and by proving the idea that it serves as a depollutant for water treatment. Finally, understand well the chemical interactions that occur between the produced substance and metal cations. The efficiency of the materials synthesized for the retention of the targeted metal cations was evaluated using a variety of parameters, including equilibrium time, water pH effect, adsorbent quantity effect, and adsorbate concentration impact.

2 Experimental Section

2.1 Chemicals

Graphite powder, ferric chloride $FeCl_3$, sodium nitrate $NaNO_3$, sulfuric acid H_2SO_4, potassium permanganate $KMnO_4$, hydrogen peroxide H_2O_2, hydrochloric acid HCl, and the bases used, such as sodium hydroxide NaOH and potassium KOH, were purchased from Sigma Aldrich. They were used in adequate concentrations. Distilled and deionized water were the main solvents for dilution and washing.

2.2 Preparation of Graphene Oxide GO

Graphene oxide GO was prepared according to the modified Hummer method, by chemical oxidation of graphite to give graphite oxide. This method is based on two main steps: chemical oxidation of graphite to give graphite oxide and exfoliation of the latter by sonication in water to obtain exfoliated graphene oxide nanosheets. For this purpose, 2 g of graphite and 1 g of sodium nitrate $NaNO_3$ were mixed with 46 mL of sulfuric acid H_2SO_4 and stirred for 1 h in an ice bath. Then, with vigorous stirring, 6 g of $KMnO_4$ was slowly added in an ice bath, so that the temperature of the mixture remained below 5 °C. After stirring the solution for 2 h at a temperature of 35 °C, 30 mL of distilled water was slowly added, giving an exothermic reaction, allowing the solution to reach a temperature of 95 °C [35, 50, 51].

The solution was stirred for 30 min at 95 °C to complete the reaction. The solution was diluted with distilled water (75 mL) and treated with a hydrogen peroxide (30% H_2O_2, drop by drop) solution to reduce the residual permanganate to soluble manganese ions until the evolved gas stopped. Finally, the mixture was filtered, after cooling in air, to give a pasty product of yellow–brown color.

The graphite oxide solution is subjected to ultrasonic treatment for 30 min in order to exfoliate the layers of graphite oxide and obtain graphene oxide (GO). The latter was centrifuged and washed with HCl solution (37%), and then with distilled water (several times). Graphene oxide is dried for 24 h at 60 °C.

2.3 Preparation of Magnetized Graphene Oxide α-Fe_2O_3/GO

To begin, a 0.5 M aqueous solution of the ferric chloride $FeCl_3$ was prepared and left to stir for 3 h until a homogeneous solution was obtained. Another aqueous GO solution

(1 g of GO in 100 mL of H_2O) was left under sonication for 100 min until a uniform solution was obtained [52, 53].

The GO solution was gradually added to the first solution 1:1 (v/v). Subsequently, a concentrated aqueous solution of NaOH was slowly added (drop by drop) to the previous solution with stirring until the pH value was around 11. Alkaline solutions like NaOH and KOH have been used, to promote the precipitation of metallic precursors [52, 54].

The resulting solution was vigorously stirred for 30 min before being placed in an autoclave for 3 h of hydrothermal treatment at 180 °C.

2.4 Characterization

A spectrometer of the brand FTIR-ATR (Alpha-Brucker) was used to characterize the synthesized materials in the range of mid-infrared wave numbers, between 400 and 4000 cm^{-1}. This instrument runs on Opus 6.5 software and comes with a tough diamond crystal total reflectance (ATR) attachment that allows for useful analysis without the usage of KBr pellets.

A Bruker Senterra dispersive Raman spectrometer with a 785 nm laser beam as the light source and a 10 mW excitation power was used for the Raman investigations.

Scherrer and Williamson-Hall based X-ray diffraction is based on the recording of a diffractogram, which makes it possible to identify and quantify the phases, calculate the crystallographic parameters and determine the average size of the crystallites by different methods (Scherrer, Williamson-Hall). Our samples were analyzed using a Bruker D8 Advance Eco diffractogram with a copper tube (= 1.54).

The concentration of metal cations was measured using a Shimadzu UV-2401 PC spectrophotometer. The 3,6-bis (2-arsenazophenylazo)-4,5 dihydroxynaphtalene-2,7-disulphonique acid, also known as Arsenazo(III), was used for molecular absorption spectroscopy. The latter is particularly well suited for UV–visible measurement of cadmium and lead ions [55–57], as well as certain other elements.

The Brunauer–Emmett–Teller (BET) method was used to determine the specific surface and pore size. The measurements are recovered through N_2 adsorption and desorption at 77 °K, and the data is collected and processed by Quanta Chromium Autosorb-6.

Cd^{2+} and Pb^{2+} calibrations were performed with standard solutions with concentrations ranging from 10^{-3} to 5.10^{-5} mol/L. Calibration curves (absorbance according to concentration) obtained from linear regression of experimental points have shown good linearity at 600 cm^{-1} wavelength (Cd^{2+}) and 650 cm^{-1} (Pb^{2+}). The regression coefficients of Cd^{2+} and Pb^{2+} are, respectively, 0.98 and 0.97. The accuracy and precision of the instrument were determined by measuring the absorbance against the prepared standard in the concentration range.

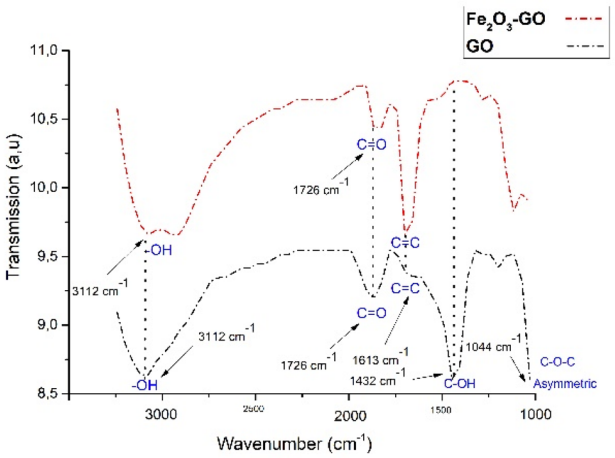

Fig. 1 ATR-FTIR spectra of GO and α-Fe_2O_3/GO

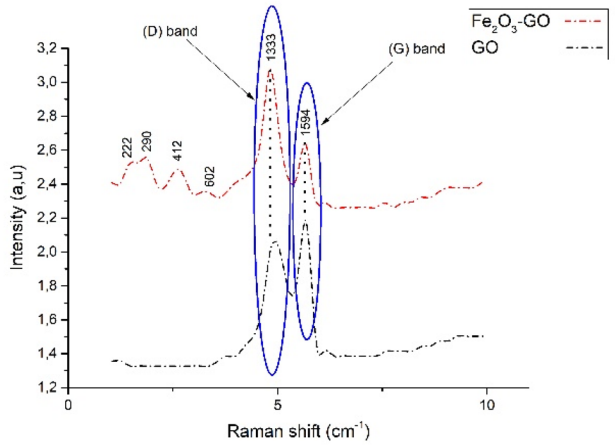

Fig. 2 Raman spectra of GO and α-Fe_2O_3/GO

3 Results and Discussion

FTIR spectra were used to investigate the vibration modes of functional groups of GO or the α-Fe_2O_3/GO composite (shown in Fig. 1). The GO curve shows the C=O stretch vibration (1726 cm^{-1}), the –OH bend vibration and C=C stretch vibration (1613 cm^{-1}), the C–OH bend vibration (1432 cm^{-1}), and the epoxy or alkoxy C–O stretch vibration (1044 cm^{-1}) [58, 59]. Other weaker peaks in the FTIR spectra of the α-Fe_2O_3/GO composite, such as the C–O functional groups of GO, are also visible, showing that the α-Fe_2O_3 nanoparticles are anchored to the GO sheets [60, 61].

The presence of α-Fe_2O_3 and GO in the α-Fe_2O_3/GO composite was confirmed using Raman spectroscopy. Figure 2 shows two typical peaks at 1333 cm^{-1} and 1594 cm^{-1} for the GO (the D band signifies disorder carbon) (the G

band represents graphitic carbon), respectively. In carbon materials, the intensity ratio of these two bands (ID/IG) can be utilized to determine the degree of structural laws and disorder [62]. This ratio was higher in the α-Fe_2O_3/GO composite (ID/IG = 1.3) than in the GO (ID/IG = 0.99). This implies that the α-Fe_2O_3/GO composite has grown more disordered, as well as confirming that the GO has become partially reduced due to the presence of iron [63]. The low wave number range (400–1000 cm^{-1}) was fine scanned to further establish the development of the α-Fe_2O_3/GO composite; the two broad bands at 412 cm^{-1} and 602 cm^{-1} can be seen in Fig. 2, and they belong to α-Fe_2O_3.

The XRD patterns of the GO and α-Fe_2O_3/GO composite are shown in Fig. 3. As illustrated, a diffraction peak of GO was found at 2θ = 11°, corresponding to an interlayer spacing (d) of 8 Å with Miller indices (001) [64]. At 2θ = 28°, another large diffraction peak was discovered, corresponding to an interlayer spacing of around 2.9 Å with Miller indices of (002).

The XRD patterns of as-prepared α-Fe_2O_3/GO composite. The peaks at 2θ = 31°, 46°, 53°, 63° and 96° are respectively indexed as the (012), (104), (110), (024) and (116) [65–67]. The intercalation of α-Fe_2O_3 nanoparticles in GO prevented the restacking of GO layers, hence the characteristic peak for GO was not identified in the α-Fe_2O_3/GO composite.

The nitrogen adsorption/desorption isotherms for the prepared α-Fe_2O_3/GO material are shown in Fig. 4. The isotherm emphasizes the mesoporous character of these materials by having the same shape (IV) as the IUPAC classification and systematic hysteresis [68, 69]. In Table 1, associated parameters such as special surface area (S_{BET}), and pore size are also presented.

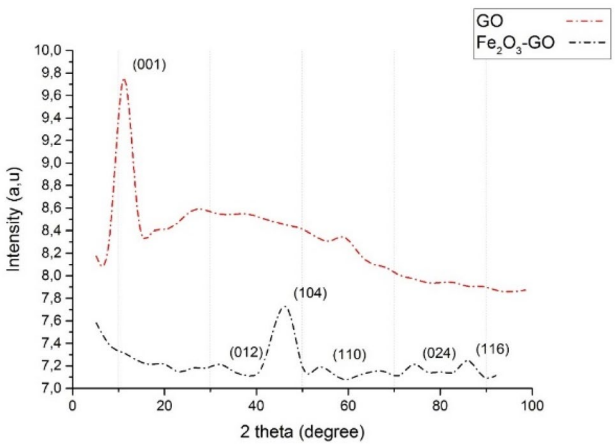

Fig. 3 XRD spectra of GO and α-Fe_2O_3/GO

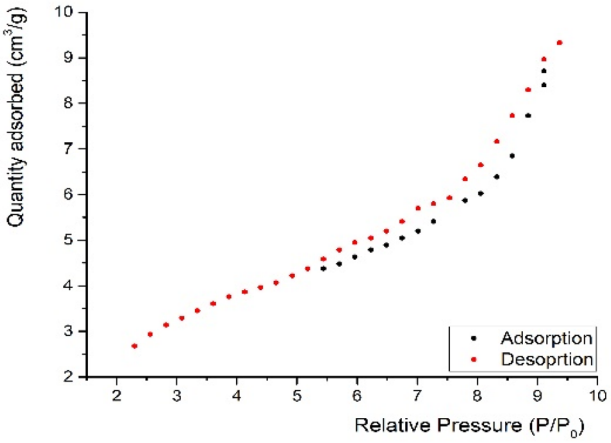

Fig. 4 BET isotherm pattern α-Fe_2O_3/GO

3.1 Adsorption Experiments

3.1.1 Equilibrium Time

As illustrated in Fig. 5, After 110 min of reaction between magnetized graphene oxide (α-Fe_2O_3/GO) and metal ions (10^{-3} M, Cd^{2+} and Pb^{2+}), 67% of the Cd^{2+} ions were retained and the elimination capacity corresponding to that was 75.12 mg/g. The Pb^{2+} ions have a nearly identical elimination rate, but it took 205 min. The adsorption peak of the two ions decreased after it reached a maximum, indicating that there is adsorption followed by desorption under the influence of agitation [70–72]. Despite the relatively low rate, the goal of this work has been achieved. Adsorption–desorption in 300 min with simple adsorbent recovery.

3.1.2 Influence of Solution pH

As long as various metal ions and the surface charge of the adsorbent are affected by pH [73, 74], the solution pH was important in the adsorption of Cd^{2+} and Pb^{2+} on GO and α-Fe_2O_3/GO. Figure 6 depicts the adsorption efficiency of Cd^{2+} and Pb^{2+} solutions (100 mg/L) at pH 4.0, 6.0, and 8.0. For this the solutions pH were adjusting with 0.1 mol/L HCl and 0.1 mol/L NaOH, and the pH range was from 4 to 8. The two metal cations Cd^{2+} and Pb^{2+} appear to have been maintained in substantial percentages (86% and 75% respectively) by the α-Fe_2O_3/GO at pH 6 after 150 min of stirring.

Table 1 Brunauer–Emmett–Teller (BET) parameters for Fe_2O_3/GO and GO

Sample	Surface area (m^2/g)	Pore size (nm)
GO	51	15.2
α-Fe_2O_3/GO	72	12.9

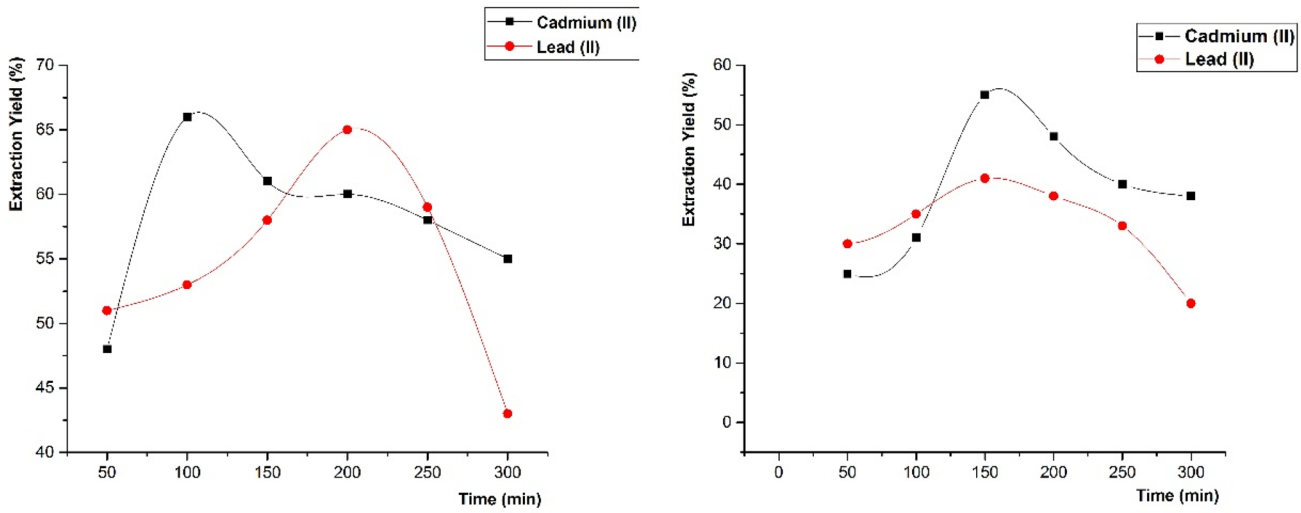

Fig. 5 Equilibrium time

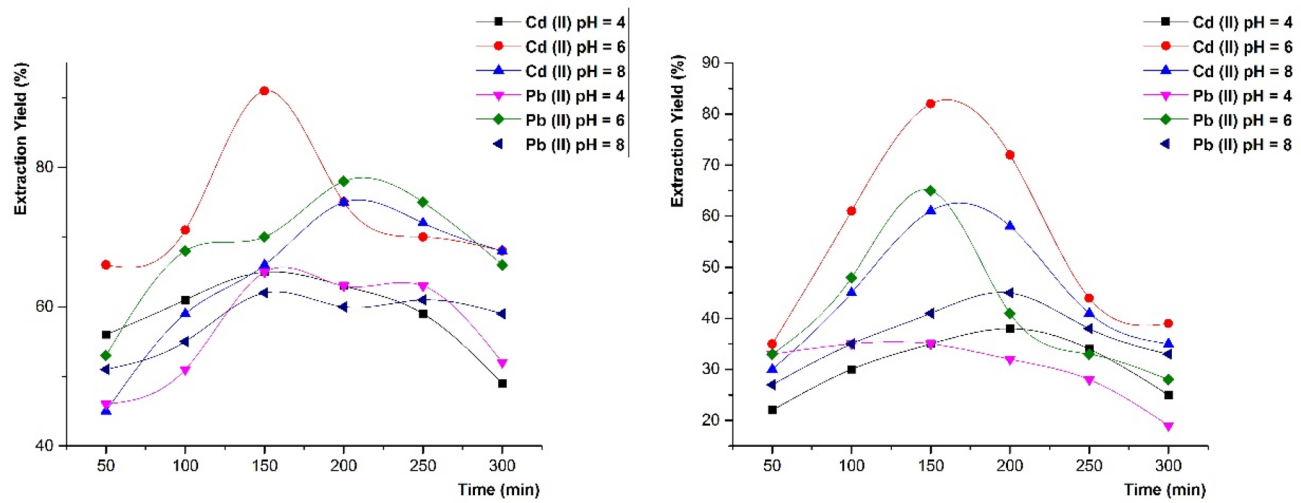

Fig. 6 pH effect

These results are remarkably similar to those obtained with the GO at pH 6.

3.1.3 Effect of the Initial Concentration of Cd^{2+} and Pb^{2+}

The study of this effect is critical for understanding the phenomenon of adsorption, particularly the adsorbent/adsorbate ratio. Figure 7 shows the rate of retention of metallic cations (Cd^{2+} and Pb^{2+}) by α-Fe_2O_3/GO and GO increases as concentration decreases and decreases as concentration of cationic pollutants increases [75]. This is perfectly reasonable, adsorption sites are largely sufficient to fix the maximum amount of Cd^{2+} and Pb^{2+} at low concentrations. Consequently, at high concentrations, these sites become saturated, reducing the percentage of adsorption [76]. The best yield achieved is more than 90% for Cd^{2+} on α-Fe_2O_3/GO and 55% for Pb^{2+} on the same adsorbent. Extraction yields with GO are nearly identical to those obtained with α-Fe_2O_3/GO.

3.1.4 Effect of Amount of Adsorbent

The amount of adsorbent has a substantial impact on the adsorption study, particularly the cost of the process [77, 78]. For this purpose, the effect of adsorbent dosage was investigated, and the results are given in Fig. 8. A sufficient amount of adsorbent results in a higher extraction yield and vice versa. Possibly, this is due to an increment

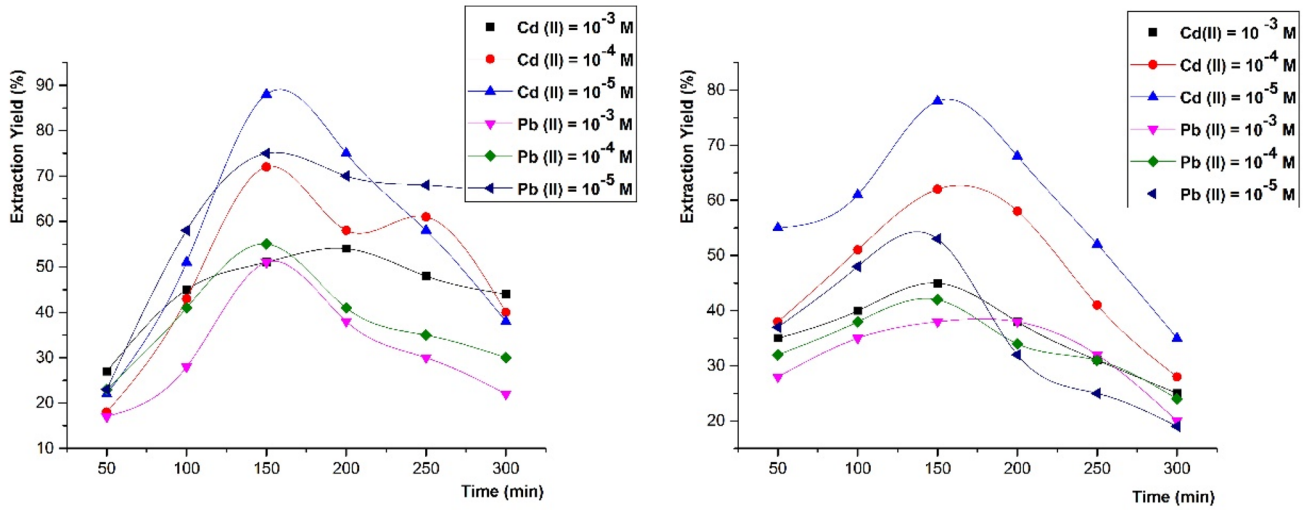

Fig. 7 Effect of the initial concentration of Cd^{2+} and Pb^{2+}

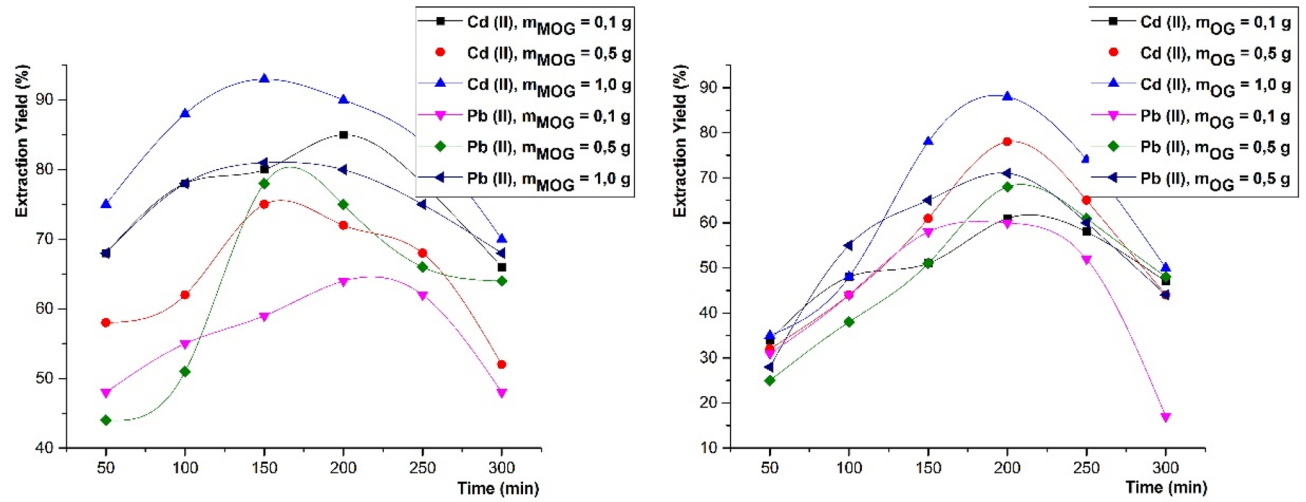

Fig. 8 Effect of the amount of the α-Fe_2O_3/GO and GO

in the number of active sites on the outer layer of the adsorbent [79, 80].

3.2 Adsorption Isotherm

Adsorption isotherms describe the distribution of adsorbate species between liquid and adsorbent through linearly plotted graphs based on a set of assumptions related to the heterogeneity or homogeneity of adsorbents [81]. In this study, Freundlich and Langmuir isotherms were studied to describe the process of adsorption of Cd^{2+} and Pb^{2+} onto α-Fe_2O_3/GO.

3.2.1 Langmuir Isotherm

The Langmuir isotherm is possibly the most important and widely used equation for describing adsorption equilibrium. This model explains the variation of adsorption of molecules (adsorbates) at a constant temperature [81]. The adsorption energy is uniform in this isotherm, and there is no migration or interaction between adsorbate molecules in the surface plane. The linear form of the Langmuir model is as follows.

$$\frac{1}{q_e} = \frac{1}{q_m * b} * \frac{1}{C_e} + \frac{1}{q_m} \quad (1)$$

q_e denotes the amount of metal cation adsorbed per unit weight of adsorbent (mg/g), where C_e denotes the equilibrium concentration of Cd^{2+} and Pb^{2+} in the solution (mg/L). q_m is the amount of Cd^{2+} and Pb^{2+} required to form a monolayer (mg/g), and b is a constant related to adsorption energy (L/mg) that represents adsorption enthalpy and should vary with temperature. The slope and intercept of line plots (Fig. 9) of $1/q_e = f(1/C_e)$ at different temperatures were used to calculate b and q_m values. By plotting a line graph of $1/q_e$ as a function of $1/C_e$. The slope of the line and the point of intersection with the y-axis can be used to calculate the values of q_e and b.

Figure 9 shows that the curve $1/C_e$ as a function of $1/q_e$ is a straight line with a correlation coefficient ($R^2 = 0.9918$, 0.9847) and an intersection (b = 12.099, 0.2831) for Cd^{2+} and Pb^{2+} respectively.

3.2.2 Freundlich Isotherm

Freundlich proposed an empirical relationship between pressure and the extent of adsorption (the amount of mass adsorbed per unit mass of adsorbent). Freundlich's equation, also known as Freundlich's adsorption isotherm, describes this relationship and explains the type I adsorption isotherm [82]. The linear equation of the Freundlich model can be represented as

$$Log\ q_e = Log\ K_f + \frac{1}{n} Log\ C_e \tag{2}$$

The intercept and slope of the plot log C_e as a function of log q_e can be used to calculate the values of parameters K_f and n ($K_f = -0.449, -1.172$) (n = 1.233, 5.602) ($R^2 = 0.761$, 0.977) Fig. 10.

According to the correlation coefficients of the two models (Table 2), Langmuir ($R^2 = 0.9918$) and Freundlich ($R^2 = 0.761$), it is clear that the adsorption of Cd^{2+} and Pb^{2+} on α-Fe_2O_3/GO follows the Langmuir model.

In order to confirm the results obtained from the two isotherms studied, we proceeded to a non-linear adjustment of the isotherm equations [83, 84] called SSE values (Eq. 3)

$$\sum_{i=1}^{n} (q_{e,cal} - q_{e,exp}). \tag{3}$$

Cadmium (Cd^{2+}) and lead (Pb^{2+}) isotherm data were best fitted by the Langmuir isotherm model with SSE < 0.010 and SSE ˂ 0.13, respectively.

3.3 Adsorption Kinetics

The most important parameter in an adsorption study is adsorption kinetics, which determines the rate of adsorption. It depends on three parameters: the complexity of the adsorbent surface, the concentration of the adsorbate, and the flow rate [85, 86]. Pseudo-first-order, pseudo-second-order, Elovich, and Intra-Particle models are among those that predict the adsorbent/adsorbate interaction [87, 88]. The first two models are commonly used in adsorption studies. Adsorption kinetics were investigated by dissolving 2 mg of adsorbent (GO and α-Fe_2O_3/GO) in 25 mL of metal ion solutions (Cd^{2+} and Pb^{2+}) at 10^{-3} mol/L concentrations. The concentration of metal ions in the vials was continuously measured at predetermined time intervals Fig. 11. The kinetics of Cd^{2+} and Pb^{2+} adsorption on α-Fe_2O_3/GO and GO can be described by the pseudo-second-order model with $R^2 = 0.993$ and $R^2 = 0.997$,

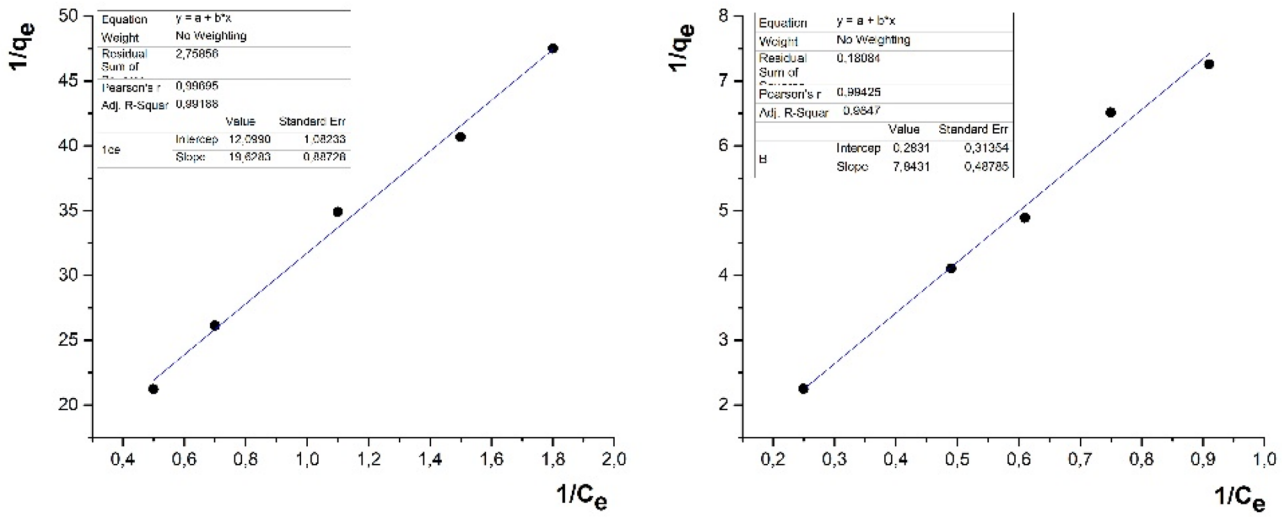

Fig. 9 Langmuir adsorption isotherm (Cd^{2+} in the left and Pb^{2+} in the right)

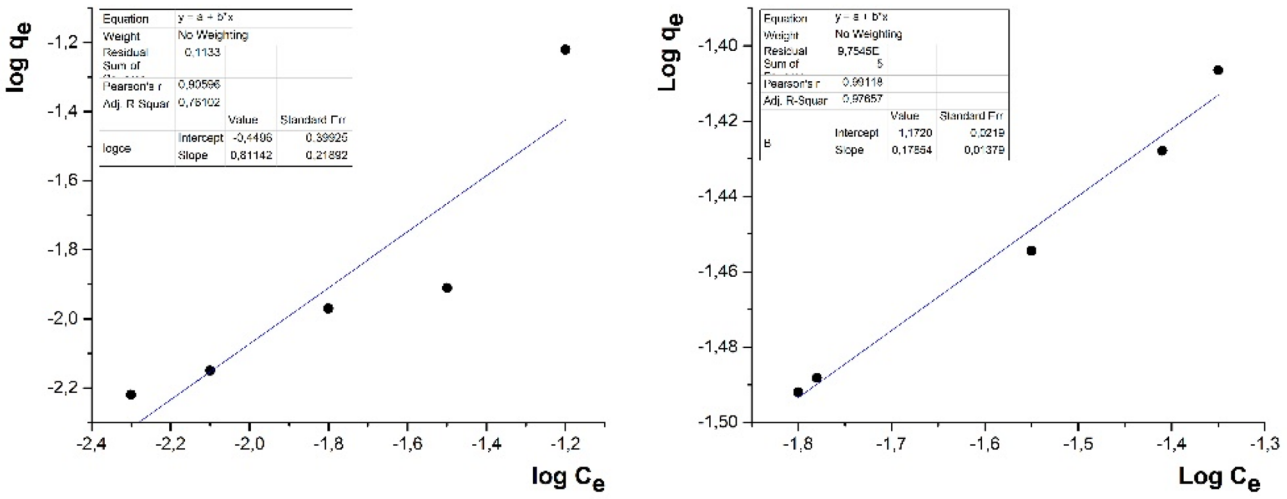

Fig. 10 Freundlich adsorption isotherm (Cd^{2+} in the left and Pb^{2+} in the right)

Table 2 The adsorption isotherm parameters and correlation coefficients (R^2)

Isotherm	Equation	Parameters		R^2
Langmuir	$\frac{1}{q_e} = \frac{1}{q_m * K_l} * \frac{1}{C_e} + \frac{1}{q_m}$	Cd^{2+}	$K_l = 0.617$ L/mg $q_m = 83.3$	$R^2 = 0.9918$
		Pb^{2+}	$K_l = 0.036$ L/mg $q_m = 35.5$	$R^2 = 0.9847$
Freundlich	$Log\ q_e = Log\ K_f + \frac{1}{n} Log\ C_e$	Cd^{2+}	$K_f = 0.638\ g^{-1}$ $1/n = 1.232$	$R^2 = 0.7610$
		Pb^{2+}	$K_f = 0.309\ g^{-1}$ $1/n = 5.602$	$R^2 = 0.9765$

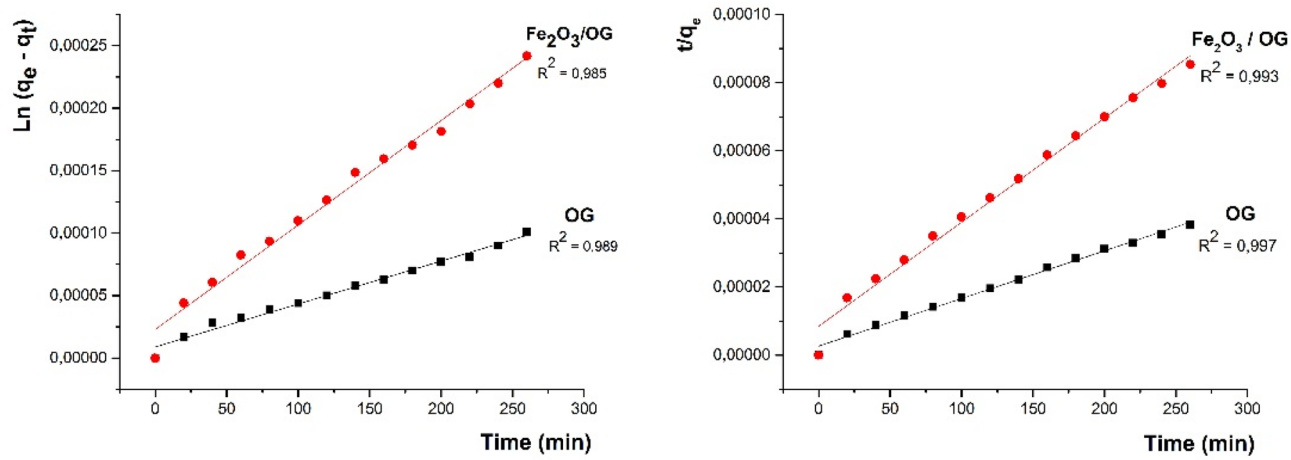

Fig. 11 Pseudo-first-order (PFO) (in left) and pseudo-second-order (PSO) (in right), kinetic models

respectively. The occupancy rate of adsorption sites is assumed to be proportional to the square of unoccupied sites in this model [89, 90], and chemisorption is the step controlling the adsorption rate [91].

3.4 Thermodynamic Study

A system's thermodynamic priorities are static averages that correspond to a large number of molecules. When

a solute molecule approaches the surface, its energy decreases until it reaches a minimum at a certain distance, close to an adsorption site [92]. This minimum is known as a potential energy well or, more simply, a potential well characterized by the determination of thermodynamic parameters (ΔH, ΔS, and ΔG) of the extracted heavy metals [93]; by the application of the following thermodynamic relations at the extraction equilibrium:

$$\Delta G^0 = \Delta H^0 - T\Delta S^0 \quad (4)$$

The Gibbs adsorption energy is made up of two terms: an enthalpy term that expresses the energies of interactions between molecules and the adsorbent surface, and an entropy term that expresses the modifications and arrangement of molecules in the liquid phase on the surface [94]. The adsorbate-adsorbent system under discussion dictates the relative relevance of the two terms.

$$\Delta G^0 = -RT \ln k_d \quad (5)$$

We derive the following expression from these two equations:

$$\ln k_d = \left(\frac{\Delta S^0}{R}\right) - \left(\frac{\Delta H^0}{R}\right)\frac{1}{T} \quad (6)$$

The equation below can be used to get the equilibrium constant K_d:

$$K_d = \frac{q_e}{C_e} \quad (7)$$

The following equation was used to calculate the adsorption capacity (q) of the metal ions (Cd^{2+} and Pb^{2+}) that α-Fe_2O_3/GO and GO studied:

$$q\left(\frac{mg}{g}\right) = (C_0 - C_e).V.\frac{M}{m} \quad (8)$$

q_e: The adsorption capacity at equilibrium.

C_0: Initial metal cation concentration in mol/L.

C_e: The concentration of metal cations at equilibrium in mol/L.

V: The volume of the treated metal cation solution (10 mL).

M: Molar masses of ($Cd(NO_3)_2$,$4H_2O$) and ($Pb(NO_3)_2$,$4H_2O$).

m: The mass of the α-Fe_2O_3/GO and GO (0.1 g).

n: The number of moles (mol).

R: The ideal gas constant (R = 8.314 J/mol/K).

K_d: The Adsorbent/adsorbate partition (distribution) coefficient.

The fitted and calculated thermodynamic results are shown in Table 3.

The results obtained from the thermodynamic functions: for cadmium ions, ΔG < 0, ΔH < 0 and ΔS ˃ 0 indicate that the adsorption is spontaneous, exothermic and that the randomness increases. Whereas for lead ions, ΔG < 0, ΔH < 0 and ΔS < 0 indicate that the adsorption is spontaneous, exothermic and order increasing. Furthermore, as the temperature rose, ΔG became almost as negative. A more negative ΔG means more spontaneity. The advantageous effect of increasing temperature on adsorption may be motivated by the fact that increasing temperature facilitates the ionization of functional groups, resulting in the formation of more adsorption sites [95, 96].

According to the literature, several sorbents have been used to remove Cd^{2+} and Pb^{2+} ions from aqueous solutions. The results obtained in terms of maximum sorption capacity were compared with this study and collected in Table 4. These results tell us that, under ideal conditions, magnetic graphene oxide α-Fe_2O_3/GO exhibits good adsorption of two metal ions, particularly cadmium (Cd^{2+}), with an elimination rate of 83.3 mg/g of sorbent.

Regarding the absorption rate of lead (Pb^{2+}), it is relatively low compared to other adsorbents such as manganese oxide coated zeolite and tea waste.

4 Conclusion

In this study, the synthesis of graphene oxide GO and modified graphene oxide α-Fe_2O_3/GO was carried out and verified using various analytical techniques. The synthesized materials have been studied as adsorbent of cadmium Cd^{2+} and lead Pb^{2+} in aqueous media. A parametric, kinetic, and thermodynamic study was conducted for this purpose, and the results show that 0.1 g of α-Fe_2O_3/GO can adsorb more than 90% of the metal ions at concentrations of 10^{-3} M of

Table 3 Fit and calculation of the thermodynamic results of Cd^{2+} and Pb^{2+} adsorption by α-Fe_2O_3/GO

T (°C)	T (°K)	ΔH (KJ/mol)		ΔS (J/K mol)		ΔG (KJ/mol)		K_d	
		Pb^{2+}	Cd^{2+}	Pb^{2+}	Cd^{2+}	Pb^{2+}	Cd^{2+}	Pb^{2+}	Cd^{2+}
25	298.15	− 2.31	− 12.33	− 3.432	8.273	− 1.021	− 2.479	1.51	2.72
35	308.15	− 2.3	− 12.1	− 3.432	8.275	− 1.055	− 2.562	1.51	2.72
45	318.15	− 2.3	− 11.5	− 3.431	8.279	− 1.089	− 2.645	1.51	2.72
55	328.15	− 2.28	− 10.9	− 3.431	8.282	− 1.123	− 2.728	1.51	2.72

Table 4 Comparison of the adsorption capacity of cadmium and lead on different adsorbents

Adsorbent	Initial conditions	Q_{max} (Cd^{2+})	Q_{max} (Pb^{2+})	References
Manganese oxide coated Zeolite	Initial concentration: 0.955 mmol/L Initial pH: 5.0 Adsorbent dosage: 10 g/L Temperature: 20 °C Contact time: 200 min	–	58.2 mg/g	[97]
Grape Stalk Wastes	Initial concentration: 60 mg/L Initial pH: 6.5 Adsorbent dosage: 10 g/L Temperature: – Contact time: –	56.11 mg/g	33.12 mg/g	[98]
Green Fe_3O_4 nano-particles	Initial concentration: 20 mg/L Initial pH: 5.5 Adsorbent dosage: 5 g/L Temperature: 20 °C Contact time: 120 min	18.73 mg/g	0.16 mg/g	[99]
Tea waste	Initial concentration: 200 mg/L Initial pH: 5.5 Adsorbent dosage: 10 g/L Temperature: 20 °C Contact time: 90 min	–	46.0 mg/g	[100]
Magnetic graphene oxide α-Fe_2O_3/GO	Initial concentration: 1 mmol/L Initial pH: 6.0 Adsorbent dosage: 10 g/L Temperature: 20 °C Contact time: 120 min	83.3 mg/g	35.5 mg/g	This work

Cd^{2+} and Pb^{2+}. The kinetic study revealed that adsorption is of pseudo-second-order, which means that in this model, the occupancy rate of adsorption sites is assumed to be proportional to the square of unoccupied sites, and chemisorption is the step that controls the adsorption rate. The thermodynamic study showed that the adsorption phenomenon is spontaneous, exothermic, and random as temperature increases. Based on these findings, we can conclude that α-Fe_2O_3/GO is a promising Cd^{2+} and Pb^{2+} adsorbent in aquatic environments with a relatively simple regeneration process.

Declarations

Conflict of interest The authors have no conflicts of interest to declare. All co-authors have seen and agree with the contents of the manuscript and there is no financial interest to report.

References

1. Rabia A, Yaseen M, Mukhtar A, Klemeš JJ, Saqib S, Ullah S, Al-Sehemi AG et al (2020) Lead and cadmium removal from wastewater using eco-friendly biochar adsorbent derived from rice husk, wheat straw, and corncob. Clean Eng Technol 1:100006. https://doi.org/10.1016/j.clet.2020.100006
2. Bhatluri KK, Manna MS, Ghoshal AK, Saha P (2017) Separation of cadmium and lead from wastewater using supported liquid membrane integrated with in-situ electrodeposition. Electrochim Acta 229:1–7. https://doi.org/10.1016/j.electacta.2017.01.090
3. Cheng S, Zhao S, Guo H, Xing B, Liu Y, Zhang C, Ma M (2022) High-efficiency removal of lead/cadmium from wastewater by MgO modified biochar derived from crofton weed. Bioresour Technol 343:126081. https://doi.org/10.1016/j.biortech.2021.126081
4. Cui N, Laiye Qu, Gang Wu (2022) Heavy metal accumulation characteristics and physiological response of Sabina chinensis and Platycladus orientalis to atmospheric pollution. J Environ Sci 112:192–201. https://doi.org/10.1016/j.jes.2021.05.013
5. Ding C, Xie A, Yan Z, Li X, Zhang H, Tang N, Wang X (2021) Treatment of water-based ink wastewater by a novel magnetic flocculant of boron-containing polysilicic acid ferric and zinc sulfate. J Water Process Eng 40:101899. https://doi.org/10.1016/j.jwpe.2020.101899
6. Chyad TF, Al-Hamadani RFC, Hammood ZA, Ali GA (2021) Removal of Zinc(II) ions from industrial wastewater by adsorption on to activated carbon produced from pine cone. Mater Today Proc. https://doi.org/10.1016/j.matpr.2021.07.016
7. Huy DH, Seelen E, Liem-Nguyen V (2020) Removal mechanisms of cadmium and lead ions in contaminated water by stainless steel slag obtained from scrap metal recycling. J Water Process Eng 36:101369. https://doi.org/10.1016/j.jwpe.2020.101369
8. Li T, Yang T, Yu Z, Xu G, Han Q, Luo G, Du J, Guan Y, Guo C (2021) Trivalent chromium removal from tannery wastewater with low cost bare magnetic Fe_3O_4 nanoparticles. Chem Eng Process Process Intensif 169:108611. https://doi.org/10.1016/j.cep.2021.108611
9. Li X-D, Xin L, Rong W-T, Liu X-Y, Deng W-A, Qin Y-C, Li X-L (2021) Effect of heavy metals pollution on the composition

and diversity of the intestinal microbial community of a pygmy grasshopper (Eucriotettix oculatus). Ecotoxicol Environ Saf 223:112582. https://doi.org/10.1016/j.ecoenv.2021.112582
10. Liu T, Lawluvy Y, Shi Y, Ighalo JO, He Y, Zhang Y, Yap P-S (2021) Adsorption of cadmium and lead from aqueous solution using modified biochar: a review. J Environ Chem Eng. https://doi.org/10.1016/j.jece.2021.106502
11. Ma M, Du Y, Bao S, Li J, Wei H, Lv Y, Song X, Zhang T, Du D (2020) Removal of cadmium and lead from aqueous solutions by thermal activated electrolytic manganese residues. Sci Total Environ 748:141490. https://doi.org/10.1016/j.scitotenv.2020.141490
12. Marichamy MK, Kumaraguru A, Jonna N (2021) Particle size distribution modeling and kinetic study for coagulation treatment of tannery industry wastewater at response surface optimized condition. J Clean Prod 297:126657. https://doi.org/10.1016/j.jclepro.2021.126657
13. Masoumi H, Ghaemi A, Gilani HG (2021) Elimination of lead from multi-component lead–nickel–cadmium solution using hyper-cross-linked polystyrene: experimental & RSM modeling. J Environ Chem Eng. https://doi.org/10.1016/j.jece.2021.106579
14. Nair K, Manu SB, Azhoni A (2021) Sustainable treatment of paint industry wastewater: current techniques and challenges. J Environ Manag 296:113105. https://doi.org/10.1016/j.jenvman.2021.113105
15. Radelyuk I, Tussupova K, Klemeš JJ, Persson KM (2021) Oil refinery and water pollution in the context of sustainable development: developing and developed countries. J Clean Prod 302:126987. https://doi.org/10.1016/j.jclepro.2021.126987
16. Rezania S, Mojiri A, Park J, Nawrot N, Wojciechowska E, Marraiki N, Zaghloul NSS (2022) Removal of lead ions from wastewater using lanthanum sulfide nanoparticle decorated over magnetic graphene oxide. Environ Res 204:111959. https://doi.org/10.1016/j.envres.2021.111959
17. Rha S, Jo HY (2021) Data describing characteristics of waste foundry dust (WFD), sorbent obtained before and after batch sorption tests using As(III) and Cr(VI) aqueous solutions. Data Brief 35:106921. https://doi.org/10.1016/j.dib.2021.106921
18. Sharma MD, Krupadam RJ (2021) Adsorption-desorption dynamics of synthetic and naturally weathered microfibers with toxic heavy metals and their ecological risk in an estuarine ecosystem. Environ Res. https://doi.org/10.1016/j.envres.2021.112198
19. Stando G, Hannula P-M, Kumanek B, Lundström M, Janas D (2021) Copper recovery from industrial wastewater—synergistic electrodeposition onto nanocarbon materials. Water Resour Ind 26:100156. https://doi.org/10.1016/j.wri.2021.100156
20. Tao X, Hu X, Wen Z, Ming Y, Li J, Liu Y, Chen R (2022) Highly efficient Cr(VI) removal from industrial electroplating wastewater over Bi2S3 nanostructures prepared by dual sulfur-precursors: insights on the promotion effect of sulfate ions. J Hazard Mater 424:127423. https://doi.org/10.1016/j.jhazmat.2021.127423
21. Tran TK, Kim N, Le QC, Nguyen MT, Leu HJ, Thi KNV (2021) Electrochemical preparation and characterization of polyaniline enhanced electrodes: an application for the removal of cadmium metals in industrial wastewater. Mater Chem Phys 261:124221. https://doi.org/10.1016/j.matchemphys.2021.124221
22. Uugwanga MN, Kgabi NA (2021) Heavy metal pollution index of surface and groundwater from around an abandoned mine site, Klein Aub. Phys Chem Earth Parts A/B/C. https://doi.org/10.1016/j.pce.2021.103067
23. Vogel N, Murawski A, Schmied-Tobies MIH, Rucic E, Doyle U, Kämpfe A, Höra C et al (2021) Lead, cadmium, mercury, and chromium in urine and blood of children and adolescents in Germany—human biomonitoring results of the German Environmental Survey 2014–2017 (GerES V). Int J Hyg Environ Health 237:113822. https://doi.org/10.1016/j.ijheh.2021.113822
24. Wang C, Li T, Yu G, Deng S (2021) Removal of low concentrations of nickel ions in electroplating wastewater using capacitive deionization technology. Chemosphere 284:131341. https://doi.org/10.1016/j.chemosphere.2021.131341
25. Zamora-Ledezma C, Negrete-Bolagay D, Figueroa F, Zamora-Ledezma E, Ni M, Alexis F, Guerrero VH (2021) Heavy metal water pollution: a fresh look about hazards, novel and conventional remediation methods. Environ Technol Innov 22:101504. https://doi.org/10.1016/j.eti.2021.101504
26. Zhou H, Zhao X, Kumar K, Kunetz T, Zhang Y, Gross M, Wen Z (2021) Removing high concentration of nickel(II) ions from synthetic wastewater by an indigenous microalgae consortium with a revolving Algal Biofilm (RAB) system. Algal Res 59:102464. https://doi.org/10.1016/j.algal.2021.102464
27. Berbar Y, Hammache ZE, Bensaadi S, Soukeur R, Amara M, Van der Bruggen B (2019) Effect of functionalized silica nanoparticles on sulfonated polyethersulfone ion exchange membrane for removal of lead and cadmium ions from aqueous solutions. J Water Process Eng 32:100953. https://doi.org/10.1016/j.jwpe.2019.100953
28. D Trishitman, A Cassano, A Basile, NK Rastogi (2020) 9—reverse osmosis for industrial wastewater treatment. In: Basile A, Cassano A, Rastogi NK (eds) Current trends and future developments on (bio-) membranes. Elsevier, pp 207–28. https://doi.org/10.1016/B978-0-12-816777-9.00009-5
29. Atanassova M (2021) Solvent extraction chemistry in ionic liquids: an overview of f-ions. J Mol Liq 343:117530. https://doi.org/10.1016/j.molliq.2021.117530
30. Xiong C, Li Y, Wang G, Fang L, Zhou S, Yao C, Chen Q et al (2015) Selective removal of Hg(II) with polyacrylonitrile-2-amino-1,3,4-thiadiazole chelating resin: batch and column study. Chem Eng J 259:257–265. https://doi.org/10.1016/j.cej.2014.07.114
31. Sun Y, Lan J, Du Y, Li Z, Liao X, Du D, Ye H, Zhang TC, Chen S (2020) Efficient removal of heavy metals by synergistic actions of microorganisms and waste molasses. Bioresour Technol 302:122797. https://doi.org/10.1016/j.biortech.2020.122797
32. Kessler E (1978) The role of parenteral hyperalimentation in the management of the burnt patient. Proc Mine Med Off Assoc S A 58(426):1–9
33. Ferrucci A, Vocciante M (2021) Improved management of water resources in process industry by accounting for fluctuations of water content in feed streams and products. J Water Process Eng 39:101870. https://doi.org/10.1016/j.jwpe.2020.101870
34. Yang S-S, Chen Y-d, Zhang Ye, Zhou H-M, Ji X-Y, He L, Xing D-F, Ren N-Q, Ho S-H, Wei-Min Wu (2019) A novel clean production approach to utilize crop waste residues as co-diet for mealworm (Tenebrio molitor) biomass production with biochar as byproduct for heavy metal removal. Environ Pollut 252:1142–1153. https://doi.org/10.1016/j.envpol.2019.06.028
35. Kadari M, Makhlouf M (2021) Graphene oxide (GO): synthesis, characterization and application to the retention of mercuric ions in aqueous solutions. Mater Today Proc. https://doi.org/10.1016/j.matpr.2021.09.426
36. Khan et al., Graphene oxide/PVC composite papers functionalized with p-phenylenediamine as high-performance sorbent for the removal of heavy metal ions
37. Chaabane L, Beyou E, Baouab MHV (2021) Preparation of a novel zwitterionic graphene oxide-based adsorbent to remove of heavy metal ions from water: modeling and comparative studies. Adv Powder Technol 32(7):2502–2516. https://doi.org/10.1016/j.apt.2021.05.011
38. Jalali K, Pajootan E, Bahrami H (2019) Elimination of hazardous methylene blue from contaminated solutions by

electrochemically magnetized graphene oxide as a recyclable adsorbent. Adv Powder Technol 30(10):2352–2362. https://doi.org/10.1016/j.apt.2019.07.018
39. Mehta D, Mazumdar S, Singh SK (2015) Magnetic adsorbents for the treatment of water/wastewater—a review. J Water Process Eng 7:244–265. https://doi.org/10.1016/j.jwpe.2015.07.001
40. Xie Y, Qian D, Dongliang Wu, Ma X (2011) Magnetic halloysite nanotubes/iron oxide composites for the adsorption of dyes. Chem Eng J 168(2):959–963. https://doi.org/10.1016/j.cej.2011.02.031
41. Mak S-Y, Chen D-H (2004) Fast adsorption of methylene blue on polyacrylic acid-bound iron oxide magnetic nanoparticles. Dyes Pigm 61(1):93–98. https://doi.org/10.1016/j.dyepig.2003.10.008
42. Rashidi NH, Ibrahim WAW, Kamboh MA, Sanagi MM (2017) New magnetic graphene-based inorganic–organic sol-gel hybrid nanocomposite for simultaneous analysis of polar and non-polar organophosphorus pesticides from water samples using solid-phase extraction. Chemosphere 166:21–30. https://doi.org/10.1016/j.chemosphere.2016.09.054
43. Cushing BL, Kolesnichenko VL, O'Connor CJ (2004) Recent advances in the liquid-phase syntheses of inorganic nanoparticles. Chem Rev 104(9):3893–3946. https://doi.org/10.1021/cr030027b
44. Gradzielski M, Langevin D, Farago B (1996) Experimental investigation of the structure of nonionic microemulsions and their relation to the bending elasticity of the amphiphilic film. Phys Rev E 53(4):3900–3919. https://doi.org/10.1103/PhysRevE.53.3900
45. Gunko YK, Cristmann U, Kessler VG (2002) Synthesis and structure of the first FeII heterometallic alkoxide [(THF) NaFe(OtBu)3]2—a possible precursor for new materials. Eur J Inorg Chem 2002(5):1029–1031. https://doi.org/10.1002/1099-0682(200205)2002:5%3c1029::AID-EJIC1029%3e3.0.CO;2-X
46. Xu J, Yang H, Wuyou Fu, Kai Du, Sui Y, Chen J, Zeng Yi, Li M, Zou G (2007) Preparation and magnetic properties of magnetite nanoparticles by sol-gel method. J Magn Magn Mater 309(2):307–311. https://doi.org/10.1016/j.jmmm.2006.07.037
47. Sivashankar R, Sathya AB, Vasantharaj K, Sivasubramanian V (2014) Magnetic composite an environmental super adsorbent for dye sequestration—a review. Environ Nanotechnol Monit Manag 1–2:36–49. https://doi.org/10.1016/j.enmm.2014.06.001
48. Pourzamani H, Parastar S, Hashemi M (2017) The elimination of xylene from aqueous solutions using single wall carbon nanotube and magnetic nanoparticle hybrid adsorbent. Process Saf Environ Prot 109:688–696. https://doi.org/10.1016/j.psep.2017.05.010
49. Kyzas GZ, Deliyanni EA, Lazaridis NK (2014) Magnetic modification of microporous carbon for dye adsorption. J Colloid Interface Sci 430:166–173. https://doi.org/10.1016/j.jcis.2014.05.049
50. Shao G, Yonggen Lu, Fangfang Wu, Yang C, Zeng F, Qilin Wu (2012) Graphene oxide: the mechanisms of oxidation and exfoliation. J Mater Sci 47(10):4400–4409. https://doi.org/10.1007/s10853-012-6294-5
51. Stankovich S, Dikin DA, Piner RD, Kohlhaas KA, Kleinhammes A, Jia Y, Yue Wu, Nguyen ST, Ruoff RS (2007) Synthesis of graphene-based nanosheets via chemical reduction of exfoliated graphite oxide. Carbon 45(7):1558–1565. https://doi.org/10.1016/j.carbon.2007.02.034
52. He Y, Yi C, Zhang X, Zhao W, Yu D (2021) Magnetic graphene oxide: Synthesis approaches, physicochemical characteristics, and biomedical applications. TrAC Trends Anal Chem 136:116191. https://doi.org/10.1016/j.trac.2021.116191
53. Luo Li, Yang Y, Haipu Li Ru, Ding QW, Yang Z (2018) Size characterization of silver nanoparticles after separation from silver ions in environmental water using magnetic reduced graphene oxide. Sci Total Environ 612:1215–1222. https://doi.org/10.1016/j.scitotenv.2017.09.024
54. Chua CK, Pumera M (2014) Chemical reduction of graphene oxide: a synthetic chemistry viewpoint. Chem Soc Rev 43(1):291–312
55. Kadari M, Kaid M, Ali MB, Villemin D (2017) Selective study of elimination of Cd(II) and Pb(II) from aqueous solution by novel hybrid material. J Chin Adv Mater Soc 5(3):149–157. https://doi.org/10.1080/22243682.2017.1329027
56. Zenki M, Minamisawa K, Yokoyama T (2005) Clean Analytical methodology for the determination of lead with arsenazo III by cyclic flow-injection analysis. Talanta 68(2):281–286. https://doi.org/10.1016/j.talanta.2005.07.059
57. Rohwer H, Collier N, Hosten E (1995) Spectrophotometric study of arsenazo III and its interactions with lanthanides. Anal Chim Acta 314(3):219–223. https://doi.org/10.1016/0003-2670(95)00279-9
58. Faniyi IO, Fasakin O, Olofinjana B, Adekunle AS, Oluwasusi TV, Eleruja MA, Ajayi EOB (2019) The comparative analyses of reduced graphene oxide (RGO) prepared via green, mild and chemical approaches. SN Appl Sci 1(10):1181. https://doi.org/10.1007/s42452-019-1188-7
59. Xu C, Shi X, Ji A, Shi L, Zhou C, Cui Y (2015) Fabrication and characteristics of reduced graphene oxide produced with different green reductants. Édité par Bing Xu. PLoS One 10(12):e0144842. https://doi.org/10.1371/journal.pone.0144842
60. Abasali karaj abad Z, Nemati A, Khachatourian AM, Golmohammad M (2020) Synthesis and characterization of RGO/Fe_2O_3 nanocomposite as an efficient supercapacitor electrode material. J Mater Sci Mater Electron 31(17):14998–15005. https://doi.org/10.1007/s10854-020-04062-7
61. Sanchez JS, Pendashteh A, Palma J, Anderson M, Marcilla R (2017) Anchored Fe_3O_4 nanoparticles on RGO nanosheets as high-power negative electrodes for aqueous batteries. ChemElectroChem 4(6):1295–1305. https://doi.org/10.1002/celc.201700048
62. Wang Y, Alsmeyer DC, McCreery RL (1990) Raman spectroscopy of carbon materials: structural basis of observed spectra. Chem Mater 2(5):557–563. https://doi.org/10.1021/cm00011a018
63. Kudin KN, Ozbas B, Schniepp HC, Prud'homme RK, Aksay IA, Car R (2008) Raman spectra of graphite oxide and functionalized graphene sheets. Nano Lett 8(1):36–41. https://doi.org/10.1021/nl071822y
64. Stobinski L, Lesiak B, Malolepszy A, Mazurkiewicz M, Mierzwa B, Zemek J, Jiricek P, Bieloshapka I (2014) Graphene oxide and reduced graphene oxide studied by the XRD, TEM and electron spectroscopy methods. J Electron Spectrosc Relat Phenom 195:145–154. https://doi.org/10.1016/j.elspec.2014.07.003
65. Biswal S, Bhaskaram DS, Govindaraj G (2020) α-Fe_2O_3/reduced graphene oxide nanocomposite: interfacial effect on the magnetic property. J Supercond Novel Magn 33(6):1629–1632. https://doi.org/10.1007/s10948-019-05211-8
66. Biswal S, Bhaskaram DS, Govindaraj G (2018) Graphene oxide: structure and temperature dependent magnetic characterization. Mater Res Express 5(8):086104. https://doi.org/10.1088/2053-1591/aad1cf
67. Bhowmik RN, Saravanan A (2010) Surface magnetism, morin transition, and magnetic dynamics in antiferromagnetic α-Fe_2O_3 (Hematite) nanograins. J Appl Phys 107(5):053916. https://doi.org/10.1063/1.3327433
68. Mohan VB, Jayaraman K, Bhattacharyya D (2020) Brunauer–Emmett–Teller (BET) specific surface area analysis of different graphene materials: a comparison to their structural regularity and electrical properties. Solid State Commun 320:114004. https://doi.org/10.1016/j.ssc.2020.114004

69. Mercier G, Klechikov A, Hedenström M, Johnels D, Baburin IA, Seifert G, Mysyk R, Talyzin AV (2015) Porous graphene oxide/diboronic acid materials: structure and hydrogen sorption. J Phys Chem C 119(49):27179–27191. https://doi.org/10.1021/acs.jpcc.5b06402
70. Kuśmierek K, Świątkowski A (2015) The influence of different agitation techniques on the adsorption kinetics of 4-chlorophenol on granular activated carbon. React Kinet Mech Catal 116(1):261–271. https://doi.org/10.1007/s11144-015-0889-1
71. Priddy SA, Hanley TR (2003) Effect of agitation on removal of acetic acid from pretreated hydrolysate by activated carbon. Appl Biochem Biotechnol 106(1–3):353–364. https://doi.org/10.1385/ABAB:106:1-3:353
72. Khalid A, Ihsanullah MZ (2018) A comparative study on the adsorption of eriochrome black T dye from aqueous solution on graphene and acid-modified graphene. Arab J Sci Eng 43(5):2167–2179. https://doi.org/10.1007/s13369-017-2543-x
73. Ouyang D, Zhuo Y, Liang Hu, Zeng Q, Yuehua Hu, He Z (2019) Research on the adsorption behavior of heavy metal ions by porous material prepared with silicate tailings. Minerals 9(5):291. https://doi.org/10.3390/min9050291
74. Cozmuta LM, Cozmuta AM, Peter A, Nicula C, Nsimba EB, Tutu H (2012) The influence of ph on the adsorption of lead by Na-clinoptilolite: kinetic and equilibrium studies. Water SA 38:269–278
75. Z Tang, H Wu, Q Wen, L Hu (2019) Effect of adsorbent dosage to adsorbate concentration ratio on the adsorption of Cd(II) on coal gangue. In: Zhan L, Chen Y, Bouazza A (eds) Proceedings of the 8th international congress on environmental geotechnics volume 1. Environmental science and engineering. Springer, Singapore, pp 428–35. https://doi.org/10.1007/978-981-13-2221-1_45
76. Al-Shehri HS, Almudaifer E, Alorabi AQ, Alanazi HS, Alkorbi AS, Alharthi FA (2021) Effective adsorption of crystal violet from aqueous solutions with effective adsorbent: equilibrium, mechanism studies and modeling analysis. Environ Pollut Bioavailab 33(1):214–226. https://doi.org/10.1080/26395940.2021.1960199
77. Biswas S, Bal M, Behera S, Sen T, Meikap B (2019) Process optimization study of Zn^{2+} adsorption on biochar-alginate composite adsorbent by response surface methodology (RSM). Water 11(2):325. https://doi.org/10.3390/w11020325
78. Gao J, Liu Yu, Li X, Yang M, Wang J, Chen Y (2020) A Promising and cost-effective biochar adsorbent derived from Jujube Pit for the removal of Pb(II) from aqueous solution. Sci Rep 10(1):7473. https://doi.org/10.1038/s41598-020-64191-1
79. Gebreslassie YT (2020) Equilibrium, kinetics, and thermodynamic studies of malachite green adsorption onto Fig (*Ficus Cartia*) leaves. J Anal Methods Chem 2020:1–11. https://doi.org/10.1155/2020/7384675
80. Gorzin F, Abadi MBR (2018) Adsorption of Cr(VI) from aqueous solution by adsorbent prepared from paper mill sludge: kinetics and thermodynamics studies. Adsorpt Sci Technol 36(1–2):149–169. https://doi.org/10.1177/0263617416686976
81. Ayawei N, Ebelegi AN, Wankasi D (2017) Modelling and interpretation of adsorption isotherms. J Chem 2017:1–11. https://doi.org/10.1155/2017/3039817
82. Belhachemi M, Addoun F (2011) Comparative adsorption isotherms and modeling of methylene blue onto activated carbons. Appl Water Sci 1(3–4):111–117. https://doi.org/10.1007/s13201-011-0014-1
83. Adeola AO, de Lange J, Forbes PBC (2021) Adsorption of antiretroviral drugs, efavirenz and nevirapine from aqueous solution by graphene wool: kinetic, equilibrium, thermodynamic and computational studies. Appl Surf Sci Adv 6:100157. https://doi.org/10.1016/j.apsadv.2021.100157
84. Anthony ET, Ojemaye MO, Okoh AI, Okoh OO (2020) Synthesis of CeO_2 as promising adsorbent for the management of free-DNA harboring antibiotic resistance genes from tap-water. Chem Eng J 401:125562. https://doi.org/10.1016/j.cej.2020.125562
85. Iriarte-Velasco U, Álvarez-Uriarte JI, González-Marcos MP, González-Velasco JR (2014) Microcolumn adsorption studies of acid/basic dyes related to the physicochemical properties of the adsorbent. Coloration Technol 130(1):62–72. https://doi.org/10.1111/cote.12058
86. Xu Z, Cai J-G, Pan B-C (2013) Mathematically modeling fixed-bed adsorption in aqueous systems. J Zhejiang Univ Sci A 14(3):155–176. https://doi.org/10.1631/jzus.A1300029
87. William K, Serkan Emik G, Öngen A, Özcan HK, Aydın S (2019) Modelling of adsorption kinetic processes—errors, theory and application. In: Edebali S (ed) Advanced sorption process applications. IntechOpen. https://doi.org/10.5772/intechopen.80495
88. El-Nemr MA, Yılmaz M, Ragab S, El Nemr A (2022) Biochar-SO prepared from pea peels by dehydration with sulfuric acid improves the adsorption of Cr^{6+} from water. Biomass Convers Biorefin. https://doi.org/10.1007/s13399-022-02378-4
89. Avelar D, Viana F, Pires BC, Nascimento TA, Mano V, Borges KB (2017) Polyaniline-deposited cellulose fiber composite prepared via in situ polymerization: enhancing adsorption properties for removal of meloxicam from aqueous media. RSC Adv 7(21):12639–12649. https://doi.org/10.1039/C6RA27019K
90. Hokmabadi F, Zadmard R, Akbarzadeh A, Tafakori V, Jalali MR, Ahmadian G (2022) Synthesis of a New Chitosan-*p-Tert*-Butylcalix[4]arene polymer as adsorbent for toxic mercury ion. R Soc Open Sci 9(5):211223. https://doi.org/10.1098/rsos.211223
91. Korake SR, Jadhao PD (2021) Investigation of taguchi optimization, equilibrium isotherms, and kinetic modeling for cadmium adsorption onto deposited silt. Heliyon 7(1):e05755. https://doi.org/10.1016/j.heliyon.2020.e05755
92. Morrison SR (1990) Adsorption and desorption. In: Morrison SR (ed) The chemical physics of surfaces. Springer US, Boston, pp 251–295
93. Singh R, Bhateria R (2020) Experimental and modeling process optimization of lead adsorption on magnetite nanoparticles via isothermal, kinetics, and thermodynamic studies. ACS Omega 5(19):10826–10837. https://doi.org/10.1021/acsomega.0c00450
94. Bermúdez-Salguero C, Gracia-Fadrique J (2011) Analysis of Gibbs adsorption equation and thermodynamic relation between Gibbs standard energies of adsorption and micellization through a surface equation of state. J Colloid Interface Sci 355(2):518–519. https://doi.org/10.1016/j.jcis.2010.12.040
95. Horsfall JM, Spiff AI (2005) Effects of temperature on the sorption of Pb^{2+} and Cd^{2+} from aqueous solution by Caladium bicolor (Wild Cocoyam) biomass. Electron J Biotechnol 8(2):162–169. https://doi.org/10.2225/vol8-issue2-fulltext-4
96. Petrovic B, Gorbounov M, Soltani SM (2022) Impact of surface functional groups and their introduction methods on the mechanisms of CO_2 adsorption on porous carbonaceous adsorbents. Carbon Capture Sci Technol 3:100045. https://doi.org/10.1016/j.ccst.2022.100045
97. Han R, Zou W, Li H, Li Y, Shi J (2006) Copper(II) and Lead(II) removal from aqueous solution in fixed-bed columns by manganese oxide coated zeolite. J Hazard Mater 137(2):934–942. https://doi.org/10.1016/j.jhazmat.2006.03.016
98. Miralles N, Valderrama C, Casas I, Martínez M, Florido A (2010) Cadmium and lead removal from aqueous solution by grape stalk wastes: modeling of a fixed-bed column. J Chem Eng Data 55(9):3548–3554. https://doi.org/10.1021/je100200w
99. Lung I, Stan M, Opris O, Soran M-L, Senila M, Stefan M (2018) Removal of Lead(II), Cadmium(II), and Arsenic(III) from aqueous solution using magnetite nanoparticles prepared by green synthesis with Box–Behnken design. Anal Lett

51(16):2519–2531. https://doi.org/10.1080/00032719.2018.1446974
100. Amarasinghe BM, Williams RA (2007) Tea waste as a low cost adsorbent for the removal of Cu and Pb from wastewater. Chem Eng J 132(1–3):299–309. https://doi.org/10.1016/j.cej.2007.01.016